Multicopter-UAV- and car-borne repeat-pass SAR interferometry and SAR tomography with the compact Gamma SAR systems: first examples and use cases at S- and L-band

O. Frey[1,2], C. Werner[1], S. Leinss[1], T. Batt[1], R. Caduff[1],
T. Dixon[3], T. Sadeghi Chorsi[3], R. Van Alphen[3], M. Schmitt[4], M. Eitel[4],
F. Sica[4], E. Deeb[5], A. LeWinter[5], D.L. Filiano[5], C.J. Wagner[5], Z. Hoppinen[5]
[1]*Gamma Remote Sensing &* [2]*ETH Zurich, Switzerland,* [3]*University of South Florida, USA,* [4]*Universität der Bundeswehr, Germany,* [5]*Cold Regions Research and Engineering Laboratory (CRREL), USA*
Correspondence: frey@gamma-rs.ch

***Abstract*—Compact SAR systems on agile platforms such as UAVs or automobiles can fill many observation gaps left open by spaceborne synthetic aperture radar (SAR) systems, such as ground motion of north/south facing mountain slopes, applications that require shorter temporal sampling intervals, high-resolution repeat-pass SAR tomography of forested areas, or combinations of spatial resolutions and frequencies currently not available from spaceborne systems. Over the last years, we have continuously developed versatile SAR imaging systems including (1) compact and lightweight FMCW SAR systems at L-band and S-band and (2) processing software for SAR imaging and interferometric processing of SAR data acquired from UAVs and automobiles. In this paper, we present our latest technology demonstrations carried out with Gamma's FMCW SAR systems in 2024 and 2025: (1) repeat-pass SAR interferometry of a fast-moving landslide at S-band, (2) our first multicopter-UAV-borne S-band SAR imagery including repeat-pass SAR interferometric acquisitions, and (3) multicopter-UAV-borne repeat-pass SAR interferometry and first UAV-based SAR tomography results of a suburban area with trees and houses at L-band.**

I. Introduction

Spaceborne synthetic aperture radar (SAR) systems offer large spatial coverage and long time series that support a variety of applications. Yet, there are many cases and applications that require complementary observations. Such cases include ground motion of north/south facing mountain slopes, applications that require shorter temporal sampling intervals, high-resolution repeat-pass SAR tomography of forested areas, or combinations of spatial resolutions and frequencies currently not available from spaceborne systems (e.g. high-resolution imaging at (sub)-meter level at L-band), etc.

Compact SAR systems on agile platforms such as UAVs or automobiles can fill several of these observation gaps as shown in our previous work [1–4]. Our goal is to complement available spaceborne and airborne SAR systems and data with versatile SAR imaging from various observation geometries to provide a choice of frequencies, spatial resolution, temporal sampling, platform and view geometry, as required by a specific application or area of interest. As an example, a compact SAR system deployed on a multicopter UAV can serve as a demonstrator for future SAR mission concepts, or the SAR system can also be integrated into lightweight manned airborne platforms or future unmanned high-altitude pseudo-satellite (HAPS) platforms.

Fig. 1. Gamma S-band SAR system (GSSAR) with a more compact and lightweight form factor (aluminum enclosure with red heat sink) mounted on a car rack for first repeat-pass interferometry demonstration using the S-band system with 400MHz bandwidth at the landslide of Brinzauls in Switzerland. The rack also holds the previous version of the Gamma L-band SAR system (yellow pelicase enclosure), which was used to produce interferograms at L-band for comparison.

Fig. 2. Gamma L-band SAR (GLSAR) system integrated on a carbon frame, which holds the entire SAR system including the GNSS-aided inertial navigation system (Honeywell HGuide n500), SAR transmit and receive antennas, and two helix-type GNSS antennas. The entire system can be easily attached and detached to/from a vibration-decoupled central mount point of the FreeFly Alta-X UAV or a similar UAV.

In this paper, we give a brief overview of our most recent technology demonstrations carried out in 2024 and 2025 with the compact FMCW Gamma SAR systems: (1) repeat-pass SAR interferometry of a fast-moving landslide at S-band with 400MHz bandwidth—with a comparison to L-band interferometric data taken quasi-simultaneously, (2) our first octocopter-UAV-borne S-band SAR imagery including repeat-pass SAR interferometric acquisitions, and (3) our first quadcopter-based repeat-pass SAR interferometry and SAR tomography results of a suburban area with trees and houses at L-band with 200MHz bandwidth.

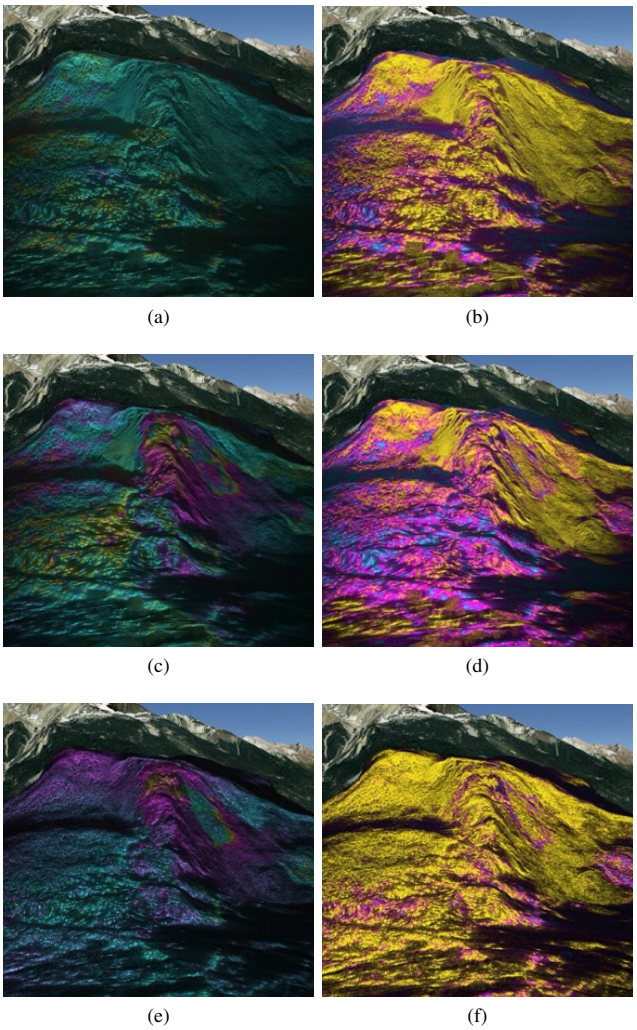

Fig. 3. Car-borne repeat-pass interferometric phase (a) and coherence (b) obtained with the Gamma S-band SAR at the landslide of Brinzauls in Switzerland for a 5-min time interval between the SAR data acquisitions. (c) and (d) show the interferometric phase and coherence for S-band SAR data for a 40-hours time interval. (e) and (f) show L-band SAR interferometric phase and coherence also for approximately the same 40-hours time interval for comparison. Color bars: see Fig. 4

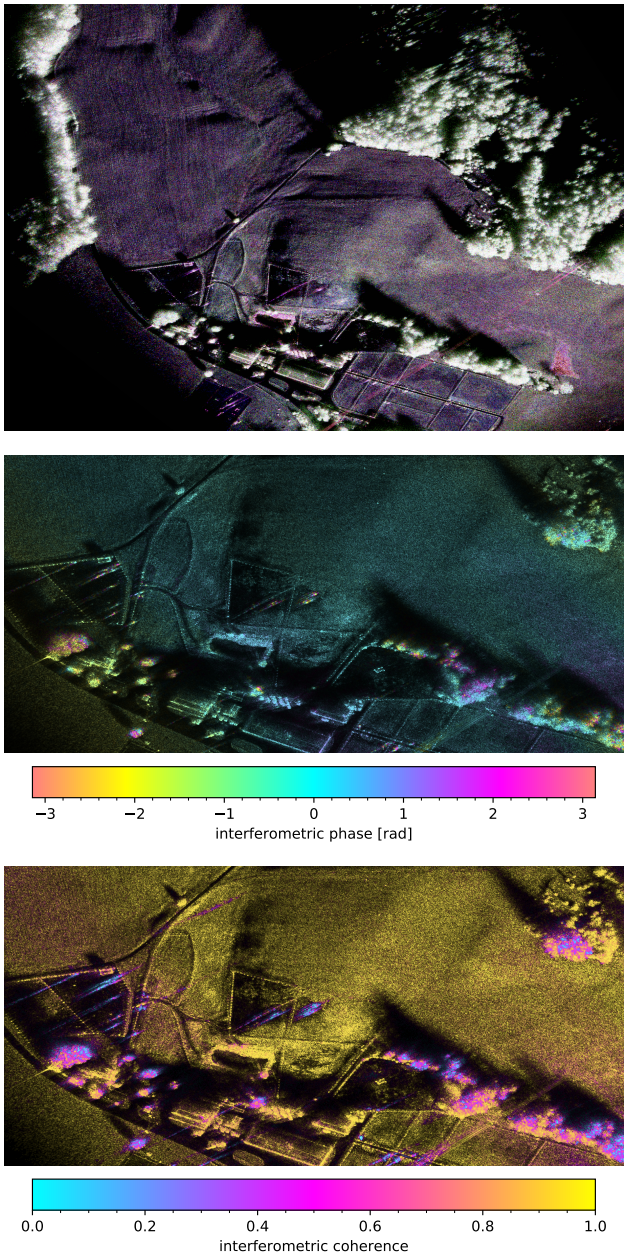

Fig. 4. Top: multicopter-UAV-borne 400MHz-bandwidth polarimetric SAR image (Pauli decomposition) acquired with the Gamma S-band SAR near CRREL, Hanover, USA, and TDBP-focused in map coordinates. Below: a zoomed view of a 7-min repeat-pass interferometric phase (middle) and coherence map (bottom).

II. Instruments, Data, and Methods

Fig. 1 shows the first version of the Gamma L-band SAR system (see [1, 3] for more details) and the more compact and lightweight new Gamma S-band SAR system, developed in 2024, mounted on a roof rack of a car at the Brinzauls landslide site[3, 4]. The Gamma S-band SAR system operates at 3.0 - 3.4 GHz providing max. resolution better than 0.5m in both range and azimuth. In Fig. 2, the new Gamma L-band SAR system mounted on a Freefly Alta-X UAV is shown. The Gamma L-band SAR systems operate at 1.2 - 1.4 GHz or at a sub-band within this frequency band. The SAR systems are equipped with GNSS/INS navigation systems. Post-processed-kinematic (PPK) GNSS data processing and GNSS/INS data fusion is employed for accurate knowledge of the sensor trajectories using a Honeywell HGuide n580/n500 system or an Applanix APX20 system together with a local GNSS reference station. Both, the Freefly Alta-X and also the Harris HX8 UAVs (the HX8 was used for the S-band UAV flights) are equipped with real-time kinematic (RTK) GNSS-aided flight control to maintain a narrow flight tube

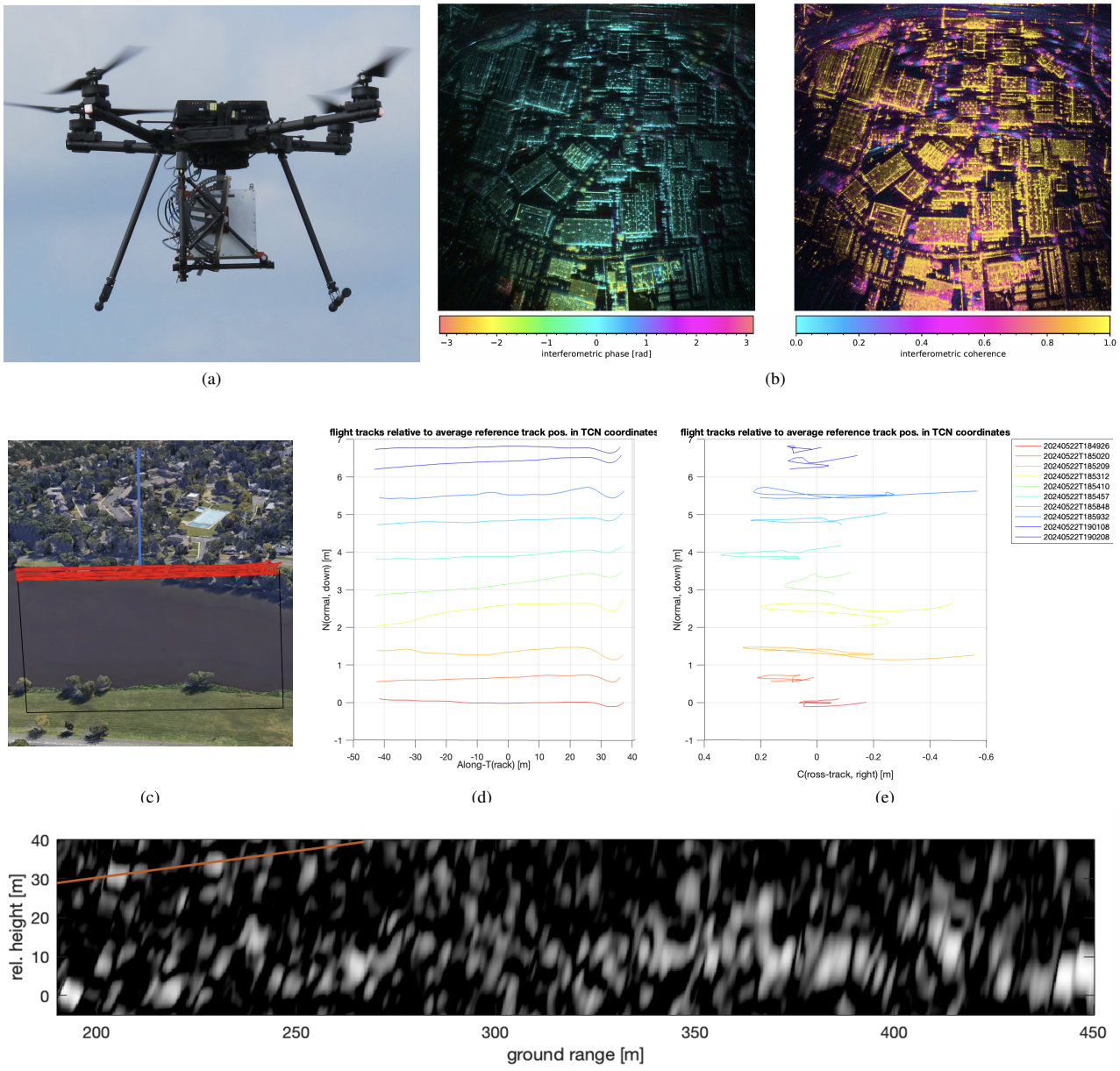

(a) (b) (c) (d) (e) (f)

Fig. 5. (a) The Gamma L-band SAR mounted on a Freefly Alta-X UAV during flight. (b) Short-term repeat-pass interferometric phase (left) and coherence (right) blended with the intensity image in the background. (c) Google earth 3-D view of the scene including repeat-pass tomographic flight tracks. (d) and (e): 10 repeat-pass tomographic acquisitions viewed in a along track (T), cross-track (C), normal (N) coordinate system (TCN) relative to a chosen reference flight track. (f) Vertical tomographic profile of SAR backscatter as obtained from tomographic imaging using the 10 repeated flight tracks that span a total vertical baseline of about 7m. The vertical profile is taken along ground range at the location as indicated with the blue line the Google Earth overview in (c). Backscatter at the different heights stems from scattering sources on the ground, from trees, and buildings that are present in the scene. The orange line on the upper-left side of tomographic profile plot (f) indicates the spatially varying height sector that can be imaged unambiguously.

around the planned trajectory. Following our previous application demonstrations including high-resolution retrieval of line-of-sight displacements of landslides [4, 5, 3, 1] we have acquired repeat-pass car-borne S-band and L-band SAR data at the Brinzauls landslide in Switzerland, in 2024. In May 2024, we had also flown a set of repeat-pass interferometric and tomographic acquisitions with the Gamma L-band SAR system mounted on a Freefly Alta-X quadcopter UAV (see Fig. 2) and, in May 2025, we have flown several repeat-pass interferometric SAR acquisitions with the Gamma S-band

SAR system mounted on a Harris HX8 octocopter drone. The UAV-borne SAR data has been focused using a time-domain back-projection (TDBP) approach [6] that we adapted for FMCW SAR data processing [7, 8] and that we implemented in C/CUDA [9] to run parallelized on an NVIDIA GPU. Likewise, the tomographic processing is obtained following the same TDBP approach with the SAR data being focused directly to a 3-D reconstruction grid in map coordinates as detailed in [10].

III. Results

In Fig. 3, S-band repeat-pass interferometric phase and coherence maps are shown as obtained from repeated car-borne SAR acquisitions with the Gamma S-band SAR (400MHz bandwidth) at the landslide of Brinzauls in Switzerland. Interferometric phase and coherence maps are shown for a very short time interval of 5 minutes (without significant displacement) and a longer time interval of about 40 hours. In addition, 40-hour interferometric phase and coherence maps of quasi-simultaneously acquired L-band SAR data are also shown for comparison. In addition, in Fig. 4, first multicopter-based S-band SAR imagery and short-term repeat-pass interferometric phase and coherence maps are shown at very high spatial resolution ($<$0.5m).

In Fig. 5, an overview of a repeat-pass interferometric campaign and a first tomographic result is shown including (a) the UAV-borne SAR system (Gamma L-band SAR mounted on a Freefly Alta-X UAV), (b) short-term, nominally zero-baseline repeat-pass interferometric phase and coherence maps of an urban area, (c)-(e) visualizations of the tomographic repeat-pass flight track configuration, and (f) a tomographic profile along ground-range showing SAR backscatter at ground level, from trees, and buildings at different height levels.

IV. Discussion

The short-term repeat-pass SAR interferogram obtained with the S-band SAR with 400MHz bandwidth shown in Fig. 3 has a clean phase and a very high coherence indicating high-quality SAR imaging without significant unknown residual positioning errors. As expected, the 40-hour interferogram shows substantial phase variations in the area of the fast-moving landslide. A high level of detail is obtained due to a range resolution better than 0.5m. For comparison a corresponding L-band interferogram is shown that has been acquired with 100MHz bandwidth. In addition to the difference in resolution, the comparison shows that the coherence level in forested areas is significantly lower at S-band (3.0-3.4 GHz) than at L-band (1.275-1.375 GHz) as expected.

The UAV-borne polarimetric S-band SAR image depicted in Fig. 4 features a high level of spatial detail; moreover, repeat-pass interferograms with good coherence were obtained. The short-term repeat-pass phase screen is rather flat (except for vegetation and buildings) with some smooth remaining phase trends that indicate residual positioning errors in the sensor trajectory, which will be further investigated in terms of the performance of the GNSS/INS navigation systems used and applicable correction approaches to further mitigate these phase trends.

The SAR tomography profile shown in Fig. 5 confirms the feasibility of multicopter-based repeat-pass SAR tomography at L-band. The number of flight tracks and the total baseline used was rather small and can be enlarged in future campaigns. A challenge for tomographic acquisitions at 100-120m above ground are the small baselines required to fulfill the height-of-ambiguity constraints. This means that real-time kinematic GNSS-based flight control of the UAV and calm wind conditions are essential to keep the UAV in a narrow flight tube.

To summarize, the multicopter-UAV-based and car-based SAR images and repeat-pass interferograms obtained with the Gamma L- and S-band SAR systems indicate that such compact SAR systems and agile sensor platforms, combined with a TDBP processing scheme, can provide high-resolution SAR images ($<$0.5m for the S-band SAR system) and support various applications that rely on repeat-pass SAR interferometry, or even SAR tomography. Potential science cases and applications include, but are not limited to, measurement of ground motion and change detection in repeat-pass interferometric mode, investigation of vegetation structure and crop growth stage, and retrieval of snowpack and ice properties or soil moisture.

References

[1] O. Frey, C. L. Werner, and R. Coscione, "Car-borne and UAV-borne mobile mapping of surface displacements with a compact repeat-pass interferometric SAR system at L-band," in *Proc. IEEE Int. Geosci. Remote Sens. Symp.*, 2019, pp. 274–277.

[2] O. Frey, C. L. Werner, A. Manconi, and R. Coscione, "Measurement of surface displacements with a UAV-borne/car-borne L-band DInSAR system: system performance and use cases," in *Proc. IEEE Int. Geosci. Remote Sens. Symp.* IEEE, 2021, pp. 628–631.

[3] O. Frey and C. L. Werner, "UAV-borne repeat-pass SAR interferometry and SAR tomography with a compact L-band SAR system," in *Proc. Europ. Conf. Synthetic Aperture Radar, EUSAR*. VDE, March 2021, pp. 181–184.

[4] O. Frey, C. Werner, and R. Caduff, "Simultaneous car-borne SAR imaging at L-band and Ku-band for DInSAR-based mobile mapping of ground motion in alpine terrain," in *Proc. of EUSAR 2024 - 15th European Conference on Synthetic Aperture Radar*. Munich, Germany: VDE, Apr. 2024, pp. 1259–1264.

[5] O. Frey, C. Werner, and R. Caduff, "Car-borne mobile mapping of ground motion by means of repeat-pass SAR interferometry: Case studies and application development based on L-band and Ku-band SAR data acquisitions," in *Proc. IEEE Int. Geosci. Remote Sens. Symp.* Pasadena: IEEE, July 2023, pp. 1902–1905.

[6] O. Frey, C. Magnard, M. Rüegg, and E. Meier, "Focusing of airborne synthetic aperture radar data from highly nonlinear flight tracks," *IEEE Trans. Geosci. Remote Sens.*, vol. 47, no. 6, pp. 1844–1858, June 2009.

[7] A. Ribalta, "Time-domain reconstruction algorithms for FMCW-SAR," *IEEE Geosci. Remote Sens. Lett.*, vol. 8, no. 3, pp. 396–400, May 2011.

[8] C. Stringham and D. G. Long, "GPU processing for UAS-based LFM-CW stripmap SAR," *Photogrammetric Engineering & Remote Sensing*, vol. 80, no. 12, pp. 1107–1115, 2014.

[9] O. Frey, C. L. Werner, and U. Wegmuller, "GPU-based parallelized time-domain back-projection processing for agile SAR platforms," in *Proc. IEEE Int. Geosci. Remote Sens. Symp.*, July 2014, pp. 1132–1135.

[10] O. Frey and E. Meier, "3-D time-domain SAR imaging of a forest using airborne multibaseline data at L- and P-bands," *IEEE Trans. Geosci. Remote Sens.*, vol. 49, no. 10, pp. 3660–3664, Oct. 2011.